Image Segmentation: An Electrostatic Field-Based Approach

Tanya Grigorishin and Yee-Hong Yang *
The Scene Analysis and Modelling Group
Computer Vision and Graphics Laboratory
Department of Computer Science
University of Saskatchewan
Saskatoon, Saskatchewan
Canada S7N 5A9
Email Address for Y.H. Yang: yang@cs.usask.ca
Phone Number for Y.H. Yang: (306) 966-4891
Fax Number for Y.H. Yang: (306) 966-4884

March 6, 1998

Abstract

Image segmentation is an important task for many problems in computer vision. Image segmentation aims at the partitioning of an image into visually distinct (homogeneous) regions.

This paper introduces a new and unique technique for image segmentation for binary and grey level images. The proposed approach relies on the Electrostatic Field Theory (EFT). Electrostatic charges are used to model the input image. The electrostatic potential is then computed and used to segment the input image. This paper entails an extensive performance evaluation and the development of the input imagery. The experimental results are very encouraging.

Keywords: electrostatic field, evaluation, image segmentation.

1 Introduction

Image processing, remote sensing, and industrial automation are the principal areas of computer vision research. These areas employ scene analysis and pattern recognition, where one uses a computer to extract high-level information from an image.

Image segmentation is one of the fundamental tasks for many problems in scene analysis and pattern recognition. It aims at the partitioning of an image into visually distinct but homogeneous regions. The homogeneity of a region can be defined by many properties, such as brightness, colour, texture, etc.

Image segmentation has found applications in different types of data such as magnetic resonance images, ultrasound images, natural and artificial textures, and synthetic aperture radar images.

The results of image segmentation are in the form of regions, the contours of which are the desired objects. A grey scale image is usually sufficient to provide information on physical discontinuities in the scene. However, colour is a useful characteristic for obtaining surface material information in a scene [21]. These material changes are interesting because they outline object entities in the image and are frequently used in object recognition.

Many techniques addressing the problem of image segmentation have been reported in the literature [11]. Many problems, however, remain unsolved. For example, methods to quantitatively evaluate the results are still lacking. Recently, there have been some efforts in this direction [17]. Many segmentation approaches fail to produce a satisfactory result for complex and noisy pictures. A number of algorithms are based on the local image properties resulting in fragmenting of regions [7]. Some techniques require human supervision to guide the segmentation process, or take into account special

*Author to whom correspondence should be addressed.
The authors would like to acknowledge Natural Sciences and Engineering Research Council of Canada for financial support through grant number OGP0000370.

characteristics of the imaging process [6].

The objective of this paper is to propose a new approach to image segmentation. The proposed approach is based on the Electrostatic Field Theory (EFT). This paper shows that the EFT presents a natural solution for the image segmentation problems.

The organisation of this paper is as follows. Section 2 introduces the EFT background. A new EFT-based approach for image segmentation is described in Section 3, which is called the EFT-based image segmentation approach. The experimental results for the EFT-based approach are discussed in Section 4. Finally, the paper concludes in Section 5.

2 Electrostatic Field Theory

This section reviews the general concepts of the EFT. For a more detailed description consult [20], [22].

1. Let us consider two charged particles separated by a fixed distance R. According to Coulomb's Law, the force acting along the line between two charges can be expressed in the following vector equation:
$$\vec{F} = C \frac{Q_1 Q_2}{R^2} \vec{r},$$
where Q_1 and Q_2 are the magnitude of charges, R is the distance between charges, C is a constant which depends on the medium, and $\vec{r}$ is a unit vector.

2. The entire region of influence of a charge is called the electrostatic field. Its magnitude is specified by a quantity called the electrostatic field intensity and is denoted by symbol E. The field intensity is defined as the force per unit charge exerted on a given charge in the field, or
$$\vec{E} = \frac{\vec{F}}{Q} = C \frac{Q}{R^2} \vec{r}.$$
The corresponding potential distribution may be found as:
$$v = C \frac{Q}{R}.$$

3. The electrostatic field intensity vector $\vec{E}(x, y)$ can be computed from the potential $v(x, y)$ as:
$$\vec{E} = -\nabla v.$$
The following observations can be made: the field is in the direction of the steepest descent of the potential; the field lines are perpendicular contours and are directed from the high to the low potential.

4. The electrostatic field conveys the same information as the curvature of an object boundary, which has been verified both theoretically and experimentally [19]. Electrostatic field extrema along an equipotential contour correspond to curvature extrema: significant convexities and concavities [1].

3 Application of EFT in Image Segmentation

In the EFT-based segmentation scheme for binary or grey level images all points of the objects are modelled as unit charges. For a binary case, the values of the charges are set to 255 (see Figure 1(a)). For a grey level image, the values of the charges are defined by the intensity values of the image points (see Figure 1(b)).

The following steps describe the organisation of the EFT-based image segmentation algorithm for binary or grey level images:

1. Compute the potential distribution $V = v(x, y)$ of image objects.

2. Detect all equipotential contours at a given potential v_{con}.

3. Display the retrieved regions.

The following sections describe the details of each of the above steps.

3.1 Solution of the Potential Distribution

The presented method of computation of the potential distribution $V = v(x, y)$ uses a predefined structuring element. The structuring element K is of the same size as the image. The origin is at the centre of the structuring element. The value of the element at location (x, y) is $\frac{1}{(x^2+y^2+depth^2)^\alpha}$, where $depth$ is an integer number that defines the viewing distance from the image plane ($depth \geq 1$), α is a real number parameter defined by the user ($\alpha \geq 0.5$).

The value of the element at location (x, y) gives the contribution of a unit charge located at (x, y) because the electrostatic potential $v(x, y)$ at the centre is inversely proportional to the distance between (x, y) and the centre of the mask. Hence, the total potential at the centre of the mask is the summation of all the potentials due to charges within the neighbourhood of the mask.

The potential distribution is given by the convolution of K with the input image, which can be

computed efficiently using the Fast Fourier Transform (FFT). The FFT of K is computed and then it is pointwise multiplied with the FFT of the input image. The inverse FFT is then performed to obtain the potential field distribution of the image.

After the potential distribution is computed, it is normalised as follows. The potentials outside the object boundaries are set equal to 0. The maximum potential is set equal to 255. The potential values inside the objects are computed using a simple linear transformation.

3.2 Tracking of Equipotential Contours

The equipotential contours at a given potential, v_{con} within the range 0 - 255, are constructed from the computed potential map. This step can be visualised as a 3D surface $V = v(x, y)$ being cut by a constant potential plane (parallel to the x-y plane). The curves that result from the intersection of the potential surface and the cutting plane are closed equipotential contours at a given potential. These equipotential contours outline the regions in the image.

The regions that correspond to the equipotential contours at a given potential are defined as follows:

$$R = \{R_1(s), R_2(s), \ldots, R_k(s), \ldots, R_n(s)\},$$

where n is the number of regions, $R_k(s) = \{(x, y) \mid v_{con} \leq v(x, y)\}$, $k = 1, 2, \ldots, n$, and $v(x, y)$ is the potential at location (x, y). The pixel values of the segmented regions are set equal to a mean value of the corresponding region pixels of the original image.

It is worth noting that the higher the value of the contour potential v_{con}, the closer the contours are located to the boundaries of the objects. Figure 2 depicts the input grey level image and some equipotential contours constructed for this image at various potentials. For the higher potential value of 240, the equipotential contours outline the central parts of the image regions. The equipotential contours at a lower potential value of 30 are located closer to the regions' boundaries. This is an interesting property, particularly for the images with severe boundary noise for the image objects.

A larger value of α reduces the influence of the charges that are located at a greater distance and increases the contribution of the neighbouring charges. Therefore, a larger value of α forces the equipotential contours to be located closer to the regions' boundaries. Figure 3 illustrates the influence of parameter α on the behaviour of the equipotential contours.

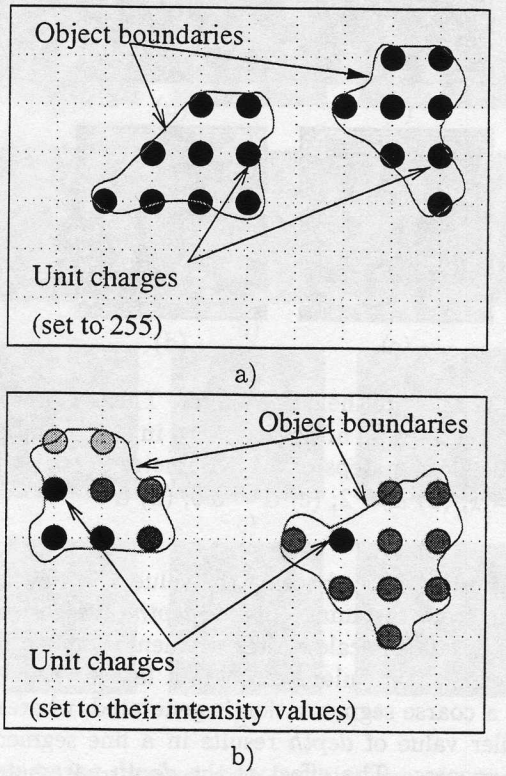

Figure 1: The EFT-based image model: (a) for a binary image; (b) for a grey level image.

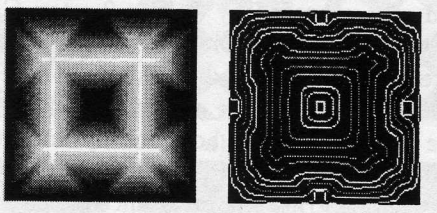

Figure 2: Distribution of the equipotential contours. (a) Original grey level image. (b) The colour contours are the equipotential contours. The equipotential contours shown are constructed in the potential range 0 - 255 in steps of 30.

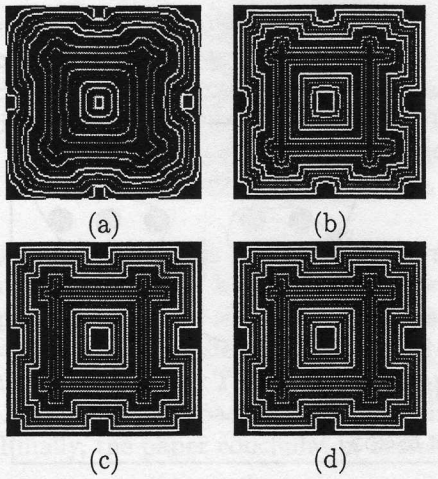

Figure 3: Effect of the α parameter. The equipotential contours shown are constructed in the potential range 0 - 255 in steps of 30, parameter *depth* = 1. (a) $\alpha = 1$; (b) $\alpha = 2$; (c) $\alpha = 3.5$; (d) $\alpha = 5$.

By appropriately choosing the value of a viewing distance from the image plane, *depth*, the desired level of detail (or scale) of the segmentation can be selected. In particular, choosing a larger value of *depth*, a coarse segmentation is generated, whereas a smaller value of *depth* results in a fine segmentation process. The effect of the *depth* parameter on the behaviour of the equipotential contours is illustrated in Figure 4.

4 Experimental Results

To test the performance of the EFT-based image segmentation the following synthesised and real images are used: 1) Binary images of a crossboard with different size parameters. Noisy images of a crossboard are generated by adding 0-mean Gaussian noise with standard deviation σ ranging from 0 to 50 in steps of 5. Figure 5 depicts some of the images in this category. Some existing segmentation techniques have a bias for horizontally and vertically oriented edges. The images of a crossboard are selected to illustrate the invariance of the EFT-based approach to the orientation of the edges in an image. 2) To generate synthesized grey level images, the distance transformation of a binary image is used as the grey level image (see Figures 6).

Evaluation is an important issue in image processing. Most algorithms are evaluated visually and qualitatively. To evaluate the performance of the EFT-based image segmentation, the F-evaluation

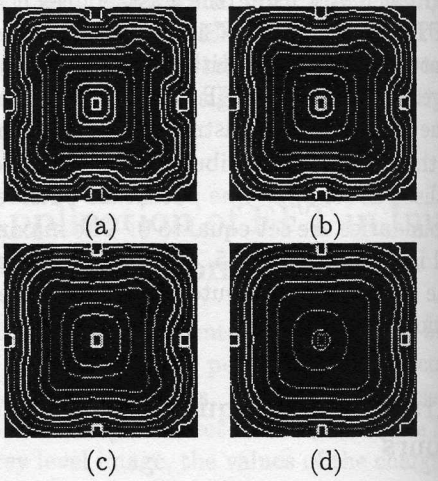

Figure 4: Effect of the *depth* parameter. The equipotential contours shown are constructed in the potential range 0 - 255 in steps of 30, parameter α = 1. (a) *depth* = 1; (b) *depth* = 3; (c) *depth* = 5; (d) *depth* = 10.

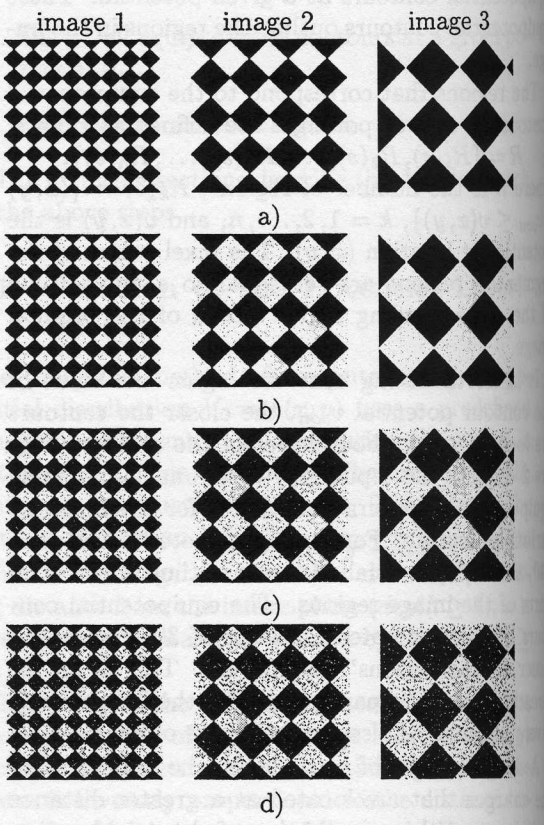

Figure 5: Binary images of a crossboard for image segmentation corrupted with 0-mean Gaussian noise with standard deviation: (a) $\sigma = 0$ (noise free); (b) $\sigma = 10$; (c) $\sigma = 30$; (d) $\sigma = 50$.

measure introduced in [16] is adopted. For the binary and grey level image segmentation the following evaluation function is used: $F(I) = \sqrt{R} \times \sum_{i=1}^{R} \frac{e_i^2}{\sqrt{A_i}}$, where I is the input binary image, R denotes the number of regions in the segmented image, e_i is the error of region i, defined as: $e_i = \sum_{j=1}^{A_i} |X1 - X2|$, where $X1$ is the value of the pixels j in the original image I and $X2$ is the assigned value of the same pixel in the segmented image.

According to [16] good segmentation results should satisfy the following criteria: regions should be homogeneous, should not contain many holes inside, adjacent regions should be significantly different and regions boundaries should be smooth. These criteria are used to judge the performance of the EFT-based approach.

To quantitatively evaluate the performance of the EFT-based approach two evaluation measures are used: the F-measure and the difference error between an ideal segmented image and a segmented image using the EFT-based approach. The image difference is defined as $D(S, I) = S - I$, where $-$ is the standard difference operation. For binary and grey level images, $S - I = \{ |s(x,y) - i(x,y)| \mid s(x,y) \in S, i(x,y) \in I \}$. The difference error is the measure that depends upon the number of pixels assigned to incorrect regions. In this paper, $D(S, I)$ is normalised by the size of an image.

First, the performance of the EFT-based approach for binary images is examined. Figures 7 and 8 illustrate the segmentation results of the images of a crossboard depicted in Figure 5. Tables 1 and 2 show the values of the F and $D(S, I)$ measures for the segmented images.

It is noteworthy that the potential values that correspond to the lowest value of the F-evaluation measure are selected in the segmentation process. All of the segmented images reflect the details of the original image. The results do not appear noisy, e.g. with many small holes in the regions. Most noise is suppresed in the result. With the increased level of noise the segmented regions have jagged boundaries, this is reflected by both evaluation measures. The jagged boundaries can be improved by appying smoothing techniques, which are not considered in this paper.

With respect to the grey level images, the segmentation results are illustrated in Figures 9 and 10. The original images are depicted in Figure 6. These original images are obtained by computing the distance transform of binary images. Tables 3 and 4

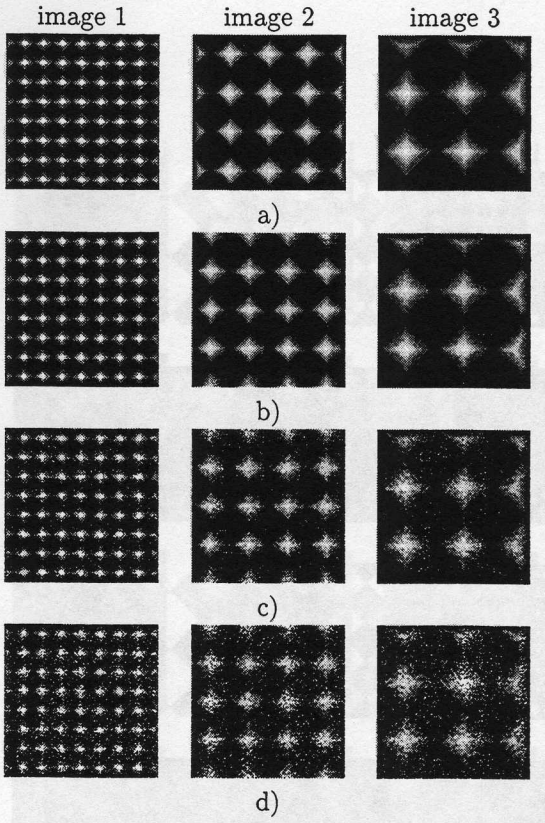

Figure 6: Synthesised grey level images of a crossboard for image segmentation generated by applying a distance transform to the binary images depicted in Figure 5(a). Images are corrupted with 0-mean Gaussian noise with variance: (a) $\sigma = 0$ (noise free); (b) $\sigma = 10$; (c) $\sigma = 30$; (d) $\sigma = 50$.

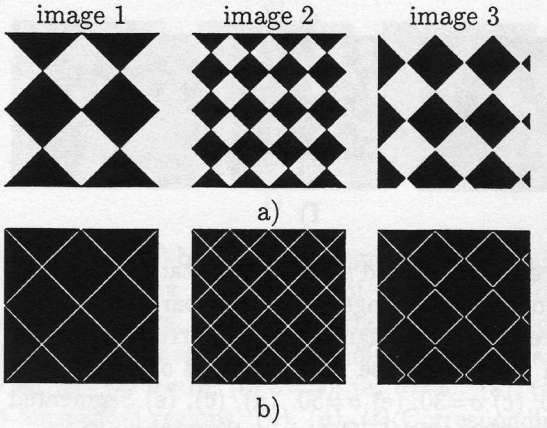

Figure 7: EFT-based image segmentation results of the noise-free binary images of a crossboard depicted in Figure 5(a). (a) Segmented regions. (b) Corresponding contours.

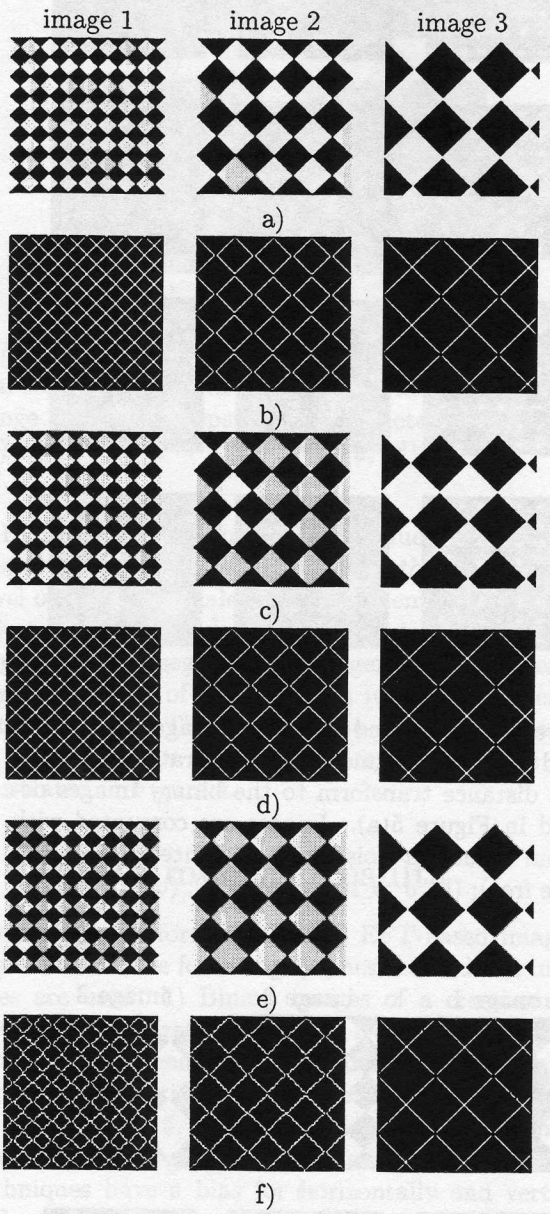

Figure 8: EFT-based image segmentation results of the noisy binary images of a crossboard depicted in Figure 5(b)-(d). Original images corrupted with 0-mean Gaussian noise with standard deviation: (a) σ=10; (c) σ=30; (e) σ=50. (a), (c), (e) Segmented regions. (b), (d), (f) Corresponding contours.

Table 1: F-evaluation measure for the binary images of a crossboard depicted in Figures 7 and 8.

Noise level (σ)	image 1	image 2	image 3
0	0	0	0
10	9.54	4.96	2.45
30	90.16	48.53	24.59
50	255.27	135.09	65.75

Table 2: $D(S, I)$ measure for the binary images of a crossboard depicted in Figures 7 and 8.

Noise level (σ)	image 1	image 2	image 3
0	0	0	0
10	3.55	3.54	3.52
30	12.24	11.57	12.00
50	20.30	19.51	19.64

show the values of the F and $D(S, I)$ measures for the segmented images.

5 Summary

In this paper a set of experiments was presented to examine the performance of the EFT-based approach under different parameters, and different levels of 0-mean Gaussian and 0-mean boundary noise. To test the performance of the approach a range of binary, grey level and colour images has been developed. The EFT-based approach has been shown to possess a number of desirable features, such as noise resistancy and a multi-scale representation.

In order to evaluate the EFT-based image segmentation results quantitatively, the F-evaluation function is used. This measure has been modified to reflect the specifics of the approach. The F-measure is used to select the potential values so the best segmentation results can be obtained. The difference errror measure has been used to study the noise sensitivity of the approach. The experimental results demonstrate the feasibility of the proposed approach.

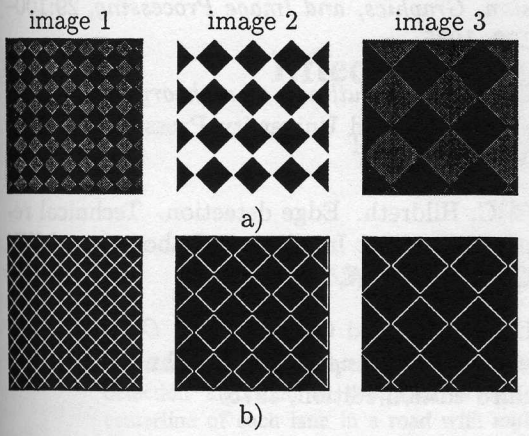

Figure 9: EFT-based image segmentation results of the noise-free grey level images of a crossboard depicted in Figure 6(a). (a) Segmented regions. (b) Corresponding contours.

Table 3: F-evaluation measure for the grey level images of a crossboard depicted in Figures 9 and 10.

Noise level (σ)	image 1	image 2	image 3
0	64.32	99.99	53.28
10	75.14	105.21	70.77
30	250.79	317.61	334.39
50	405.48	759.87	890.82

Table 4: $D(S, I)$ measure for the grey level images of a crossboard depicted in Figures 9 and 10.

Noise level (σ)	image 1	image 2	image 3
0	17.61	22.57	14.72
10	19.32	23.03	19.89
30	25.60	28.89	22.70
50	31.02	32.70	27.50

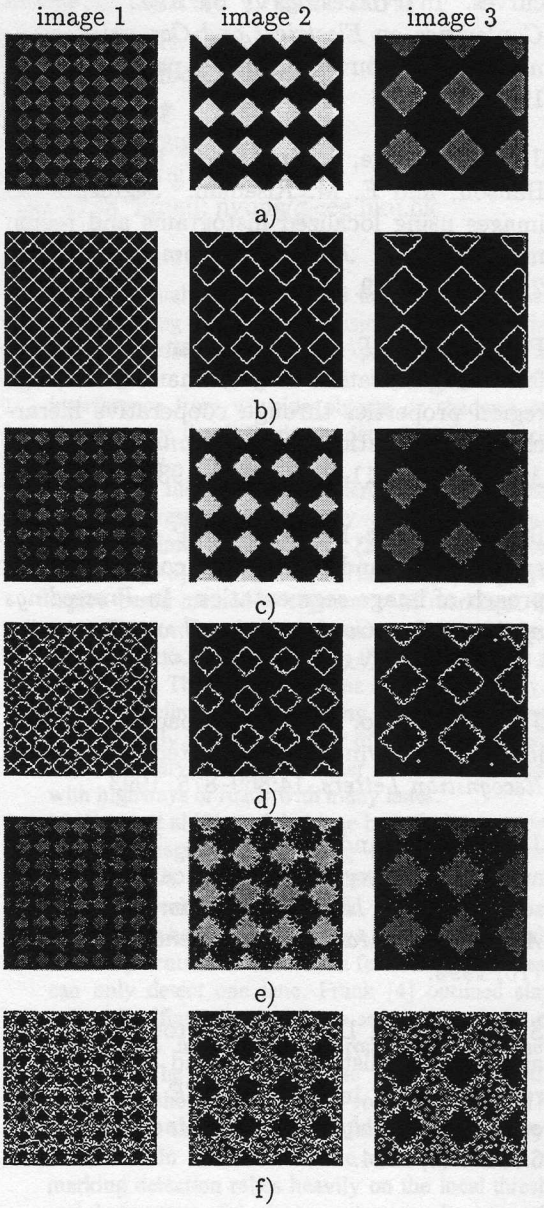

Figure 10: EFT-based image segmentation results of the noisy grey level images of a crossboard depicted in Figure 6(b)-(d). Original images corrupted with 0-mean Gaussian noise with standard deviation: (a) σ=10; (c) σ=30; (e) σ=50. (a), (c), (e) Segmented regions. (b), (d), (f) Corresponding contours.

References

[1] G. H. Abdel-Hamid and Y. H. Yang. Electrostatic field-based detection of corners of planar curves. In *Proceedings of the 1993 Canadian Conference on Electrical and Computer Engineering*, Vancouver, Canada, pages 767–770, 1993.

[2] J. R. Beveridge, J. Griffith, R. Kohler, A. R. Hanson, and E. M. Riseman. Segmentation images using localized histograms and region merging. *Int. Journal of Computer Vision*, 2:311–347, 1989.

[3] P. J. Burt, T. H. Hong, and A. Rosenfeld. Segmentation and estimation of image region properties through cooperative hierarchical computation. *IEEE Transactions Syst. Man Cybern.*, 11-12:802–809, 1981.

[4] R. K. Falah, Ph. Boloh, and J. P. Cocquerez. A region-region and region-edge cooperative approach of image segmentation. In *Proceedings of the 1st Int. Conference on Image Processing - III*, Austin, Texas, pages 470–474, 1994.

[5] J. P. Gambotto. A new approach to combining region growing and edge detection. *Pattern Recognition Letters*, 14:869–875, 1993.

[6] J. M. Gauch and S. M. Pizer. The intensity axis of symmetry and its application to image segmentation. *IEEE Transactions on Pattern Analysis and Machine Intelligence*, 15(8):753–770, 1993.

[7] S. Geman and D. Geman. Stochastic relaxation, gibbs distributions, and the bayesian restoration of images. *IEEE Transactions on Pattern Analysis and Machine Intelligence*, 6:721–741, 1984.

[8] R. Gershon. A survey on color in computational vision. Technical report, University of Toronto, Department of Computer Science, 1984.

[9] R.C. Gorzalez and P. Wintz. *Digital Image Processing.* Addison-Wesley, 1977.

[10] M. W. Hansen and W. E. Higgins. Watershed-driven relaxation labeling for image segmentation. In *Proceedings of the 1st Int. Conference on Image Processing - III*, Austin, Texas, pages 460–464, 1994.

[11] R. M. Haralick and L. G. Shapiro. Survey: Image segmentation techniques. *Computer Vision, Graphics, and Image Processing*, 29:100–132, 1985.

[12] E. Hering. *Outlines of a theory of the light sense.* Harvard University Press, Cambridge, MA, 1964.

[13] E. C. Hildreth. Edge detection. Technical report, Artificial Intelligence Laboratory, MIT, Cambridge, MA, 1985.

[14] D. B. Judd and G. Wyszecki. *Color in Business, Science and Industry.* John Wiley, N.Y., third edition edition, 1975.

[15] Khoros. *Khoros Research Inc.*, 1994.

[16] J. Liu. Multiresolution colour image segmentation. Master's thesis, Department of Computational Science, University of Saskatchewan, SK, 1993.

[17] J. Liu and Y. H. Yang. Multiresolution color image segmentation. *IEEE Transactions on Pattern Analysis and Machine Intelligence*, 16(7):689–700, 1994.

[18] David Marr. *Vision.* W. H. Freeman and Company, N.Y., 1982.

[19] R. Mittra and S. W. Lee. *Analytical Techniques in The Theory of Guided Waves.* McMillan, N.Y., 1971.

[20] A. Nussbaum. *Field Theory.* Charles E. Merrill Books, Columbus, Ohio, 1967.

[21] J. M. Rubin and W. A. Richards. Color vision and image intensities: When changes material. Technical report, Artificial Intelligence Laboratory, MIT, Cambridge, MA, 1985.

[22] P. Silvester. *Modern Electromagnetic Fields.* Prentice-Hall, N.J, 1967.

[23] J. B. Subirana-Vilanova and K. K. Sung. Multi-scale vector-ridge-detection for perceptual organization without edges. Technical report, Artificial Intelligence Laboratory, MIT, Cambridge, MA, 1992.

[24] L. Vincent and P. Soille. Watersheds in digital spaces: An efficient algorithm based on immersion simulations. *IEEE Transactions on Pattern Analysis and Machine Intelligence*, 13(6):583–598, 1991.